Icarus 314 (2018) 149–158

Contents lists available at ScienceDirect

Icarus

journal homepage: www.elsevier.com/locate/icarus

Planetary boundary layer and slope winds on Venus

Sébastien Lebonnois[*,a], Gerald Schubert[b], François Forget[a], Aymeric Spiga[a,c]

[a] Laboratoire de Météorologie Dynamique (LMD/IPSL), Sorbonne Université, ENS, PSL Research University, Ecole Polytechnique, Université Paris Saclay, CNRS, Paris, France

[b] Department of Earth, Planetary and Space Sciences, UCLA, CA, USA

[c] Institut Universitaire de France, Paris, France

ARTICLE INFO

Keywords:
Venus
Atmosphere
Planetary boundary layer
Slope winds

ABSTRACT

Few constraints are available to characterize the deep atmosphere of Venus, though this region is crucial to understand the interactions between surface and atmosphere on Venus. Based on simulations performed with the IPSL Venus Global Climate Model, the possible structure and characteristics of Venus' planetary boundary layer (PBL) are investigated. The vertical profile of the potential temperature in the deepest 10 km above the surface and its diurnal variations are controlled by radiative and dynamical processes. The model predicts a diurnal cycle for the PBL activity, with a stable nocturnal PBL while convective activity develops during daytime. The diurnal convective PBL is strongly correlated with surface solar flux and is maximum around noon and in low latitude regions. It typically reaches less than 2 km above the surface, but its vertical extension is much higher over high elevations, and more precisely over the western flanks of elevated terrains. This correlation is explained by the impact of surface winds, which undergo a diurnal cycle with downward katabatic winds at night and upward anabatic winds during the day along the slopes of high-elevation terrains. The convergence of these daytime anabatic winds induces upward vertical winds, that are responsible for the correlation between height of the convective boundary layer and topography.

1. Introduction

The interaction between the surface and the atmosphere is a key to understanding the processes driving the dynamics of both the atmosphere and the solid planet. The exchanges of heat and angular momentum drive the temperature and wind structure in the deepest layers of Venus's atmosphere, and affect Venus's atmospheric superrotation and the rotation of the planet itself. Yet, the deep atmosphere of Venus (below 10 km altitude above the surface) remains largely unexplored because of the difficulty in obtaining data below the dense and planet-wide cloud cover. Only a small number of probes have reached the surface: the Russian Venera series and VeGa missions, and the American Pioneer Venus mission. Among these probes, only one (VeGa-2) was able to measure a complete reliable temperature profile down to the surface (Linkin et al., 1986; Lebonnois and Schubert, 2017).

On Earth, the study of the planetary boundary layer (PBL) must take into account the variety of properties of the surface, and the water cycle and associated latent heat release. Its knowledge is important for a good understanding of the dispersion of trace atmospheric compounds, local circulations, clouds and water cycle or energy balance of the surface (e.g., Garratt, 1994). Arid areas are more relevant for comparative planetology since the water latent heat contribution can be neglected (e.g., Wang et al., 2016). The Martian PBL has also been studied extensively since the Viking landers (Hess et al., 1977), in particular with radio-occultation datasets and turbulence-resolving simulations (e.g., Hinson et al., 2008; Spiga et al., 2010). The surface temperature diurnal cycle is large on Mars, and the typical thickness of the diurnal convective PBL is much larger than on Earth. This PBL convective activity plays a crucial role in the dust cycle. The surface slope winds are also strong on Mars, both during daytime and nighttime. They were shown to have a significant impact on the near-surface temperature distributions (Spiga et al., 2011).

On Titan, the PBL may play a role in the near-surface methane cycle, but very few observational data are available to characterize it. The in-situ temperature profile obtained during the Huygens probe descent provided the best information to date to characterize the behavior of Titan's PBL. An interpretation of this profile and of the associated PBL characteristics was proposed by Charnay and Lebonnois (2012), based on simulations with a General Circulation Model: signatures are present of the height of the PBL at the time of the descent (300 m at 10:00 LT in the morning), of the remnant of the previous diurnal cycle, with a maximum vertical extent of the PBL of roughly 800 m, and of the height

* Corresponding author.
E-mail address: sebastien.lebonnois@lmd.jussieu.fr (S. Lebonnois).

https://doi.org/10.1016/j.icarus.2018.06.006
Received 22 December 2017; Received in revised form 1 June 2018; Accepted 4 June 2018
Available online 05 June 2018
0019-1035/ © 2018 Elsevier Inc. All rights reserved.

of the dominant surface circulation, with the seasonally-varying ascending branch (the equivalent of Earth's inter-tropical convergence zone) reaching 2 km altitude.

There have been a few attempts to investigate the surface temperatures, the PBL and the near surface winds on Venus. Surface temperatures were measured in-situ by several Venera landers (with an accuracy of ± 5 K) (Avduevskii et al., 1983) and the VeGa-2 lander (with an accuracy of ± 1 K) (Linkin et al., 1986). In addition, informations about the near-surface atmospheric temperatures can be inferred remotely from the analysis of near-infrared images in spectroscopic windows around 1.0, 1.10 and 1.18 microns. Such an analysis was done with the VIRTIS/Venus-Express datasets by Mueller et al. (2009). However, other unknown variables affect this analysis, such as the surface emissivity and the atmospheric opacities in the deep atmosphere. Disentangling all these variables is not easy, and assumptions are made that prevent a conclusive retrieval of the atmospheric lapse rate near the surface. Dobrovolskis (1983, 1993) modeled the atmospheric thermal tides induced by heating near the ground and determined wind magnitudes and directions in the PBL and the resulting surface stresses. These predictions are limited by simplifying assumptions, one of the most important being the neglect of the winds in the global circulation of the atmosphere. The PBL is affected by more than just the tidally driven winds at the surface. Several papers (Saunders et al., 1990; Greeley et al., 1991; 1994; 1995) have studied the patterns of wind streaks and aeolian transport of surface materials visible in the Magellan radar images in efforts to infer the nature of the circulation in the PBL. Greeley et al. (1994) analyzed thousands of wind streaks in the Magellan images associated with sand dunes and wind-sculpted hills. On the assumption that the streaks serve as local "wind vanes" their orientations represent a global map of near-surface wind patterns on Venus. Equatorward streaks were most dominant, consistent with a Hadley circulation of the lower atmosphere.

While waiting for additional observations, the analysis of the PBL can be investigated with the help of models. Yamamoto (2011) used a microscale model to investigate the mixing induced by convective adjustment in idealized simulations of the PBL. However, the initial conditions assumed in these numerical experiments, i.e., the potential temperature profile and the surface thermal flux, are poorly constrained by observations. In addition, the effect of the background circulation was not taken into account. Therefore, these simulations may not reflect real Venus surface conditions. Here we take a different approach, and use the latest simulations from the Venus Global Climate Model (GCM) developed at the Institute Pierre-Simon Laplace (IPSL) to investigate the convective boundary layer, characterized by the depth of the surface convective activity, and the near-surface circulation. The GCM and the simulations used are described in Section 2. The vertical structure of the potential temperature is detailed in Section 3, the temporal and spatial variability of the convective activity is investigated in Section 4. Though there are no available observations of surface winds, our simulations suggest the presence of slope winds, so they are discussed together with their impact on the near-surface thermal structure in Section 5. Conclusions are given in Section 6.

2. Model and simulations

The IPSL Venus Global Climate Model has been developed for about a decade (Lebonnois et al., 2010; 2016). It includes a full description of the radiative transfer based on the latest modeling of the solar flux (Haus et al., 2015) and infrared net exchange rates (Eymet et al., 2009) taking into account the latest latitude-dependent cloud model (Haus et al., 2014), slightly tuned to get a vertical structure of the temperature close to the available observations. The latest simulations reproduce quite well the atmospheric structure, including the cold collar and the superrotation of the atmosphere (Garate-Lopez and Lebonnois, 2018). In the deep atmosphere, the planetary boundary layer scheme used is based on Mellor and Yamada (1982), a simple but useful scheme used, e.g., to study Titan's planetary boundary layer (Charnay and Lebonnois, 2012). This scheme is detailed in Appendix B of Hourdin et al. (2002) and based on level 2.5 model described by Mellor and Yamada (1982).

The GCM physics also includes a convective adjustment scheme. In the case of an unstable situation, both the PBL mixing scheme (based on Mellor and Yamada's formulation) and the convective adjustment can act to stabilize the unstable layer. In our GCM, the PBL scheme is applied before applying the convective adjustment and therefore this adjustment rarely occurs. The PBL scheme can compute a mixing coefficient in an unstable layer even away from the surface, so it acts to mix and stabilize the layer both in the PBL near the surface and in the highly convective cloud layer, with tendencies due to convective adjustment scarcely occurring. This adjustment mostly occurs in the first two layers just above the surface, when the PBL scheme does not completely remove the unstable gradient.

The reference simulation used in this work is described in detail by Garate-Lopez and Lebonnois (2018), in particular the tuning done in the radiative transfer. The horizontal resolution is 96 longitudes by 96 latitudes, on 50 vertical levels (hybrid coordinates, from surface to roughly 95 km altitude). In the deepest 10 km, the altitudes (above surface) of the layers are located around 10, 50, 150, 370, 750 m, 1.3, 2.1, 3.2, 4.7, 6.4 and 8.5 km. It was run for 300 Venus days from an already superrotating initial state.

As proposed by Lebonnois and Schubert (2017), it is possible that the deepest 7 km of the atmosphere may not be uniformly mixed, with a vertical gradient of nitrogen, from 3.5% at 7 km altitude to almost 0% at the surface. This would have an impact on the stability of the PBL since the mean molecular mass gradient reduces the buoyancy. A simulation was performed with this gradient of mean molecular mass taken into account in order to investigate its impact on the PBL structure. Since no physical process can yet be formalized in the model to have the N_2 abundance vary, the current implementation is simple: the profile of the mean molecular mass as a function of pressure obtained from VeGa-2 analysis is used at each grid point, and the potential temperature is modified accordingly (Lebonnois and Schubert, 2017). The initial state is the reference simulation, then the simulation is run for 50 Venus days with the modified mean molecular mass profile. The impact of this hypothesis on the PBL structure is discussed in Section 4.3.

To separate purely radiative effects from dynamical ones, 1-dimensional simulations (single vertical column) were also performed at selected locations. Starting from the temperature profile obtained at a given location by the GCM simulation, the 1-dimensional runs take into account only radiative heating and cooling and local vertical turbulent mixing. At the equator, this results in a temperature profile that tends to increase slowly, since energy is not redistributed to higher latitudes by the dynamics (mean meridional circulation and planetary-scale waves). The diurnal cycles of the 1-dimensional profile and of the convection are considered after a couple of Venus days.

A caution related to surface winds needs to be mentioned. Due to angular momentum conservation problems in the GCM (as discussed in Lebonnois et al., 2016), the zonal component of the zonally and temporally averaged surface winds could be biased, in particular in low-latitude regions. Caution should therefore be taken when discussing these winds. However, we find that the diurnal variations of the surface winds are significant, with amplitudes usually larger than the average values of the zonal component. Typically, at 10 m altitude, the temporally averaged zonal wind $\overline{u}$ ranges between ± 0.15 m/s, while the temporally averaged horizontal wind $\overline{U}$ ranges roughly from 0.2 to 0.6 m/s, often a factor of 3 to 5 larger than $|\overline{u}|$ (except in polar regions). Therefore, the slope winds effects discussed in this work should be rather independent of the bias due to angular momentum conservation problems.

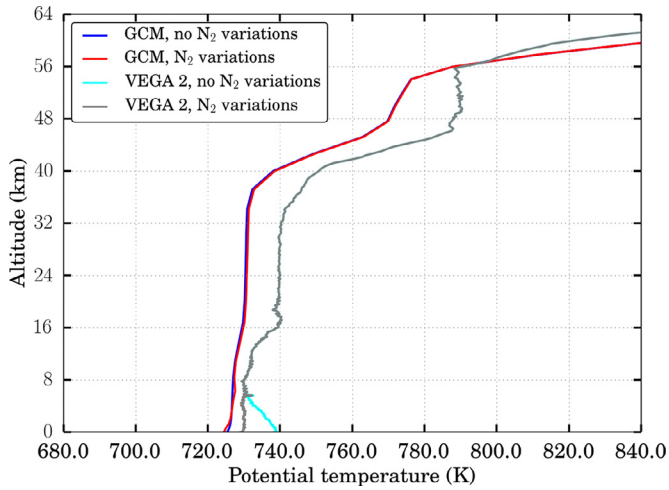

Fig. 1. Vertical profiles of potential temperature computed from the VeGa-2 temperature measurements and from the global average temperature profile of the GCM simulations, without and with N_2 abundance variations in the lowest 7 km.

3. Vertical structure of potential temperature

The deep atmosphere of Venus is structured in alternating layers of stable and well-mixed regions. Stable regions are characterized by potential temperature increasing with altitude, while well-mixed (neutral) regions have a roughly constant potential temperature. Despite recent adjustments done in the radiative transfer (Lebonnois and Schubert, 2017; Garate-Lopez and Lebonnois, 2018), the modeled temperatures are still below observed values (5 to 15 K). However, the structure obtained with the IPSL Venus GCM (Fig. 1) is in agreement with the potential temperature profiles deduced from in-situ observations by the Pioneer Venus and VeGa-2 probes (Lebonnois and Schubert, 2017): below the cloud, a stable region is present down to roughly 30 km altitude. Below this level the atmosphere is well mixed down to roughly 20 km altitude, mostly due to large-scale circulation and to very short-distance infrared radiative exchanges, according to the model that predicts little convective activity in this region. The atmosphere is stable again between 18–20 km and 8–10 km altitude. In the deepest 10 km, the atmosphere is again near neutral stability, with no convective activity predicted except in the PBL, as discussed in Section 4.

The modeled surface temperatures shown in Fig. 2 are quite

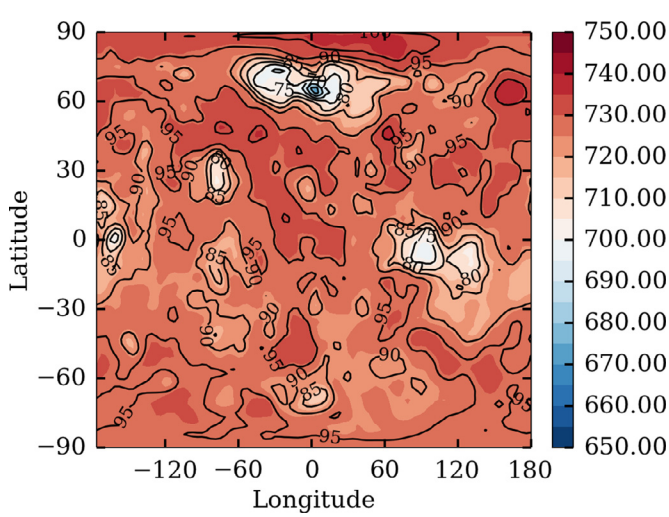

Fig. 2. Diurnally averaged surface temperature (K) with surface pressure contours (bar).

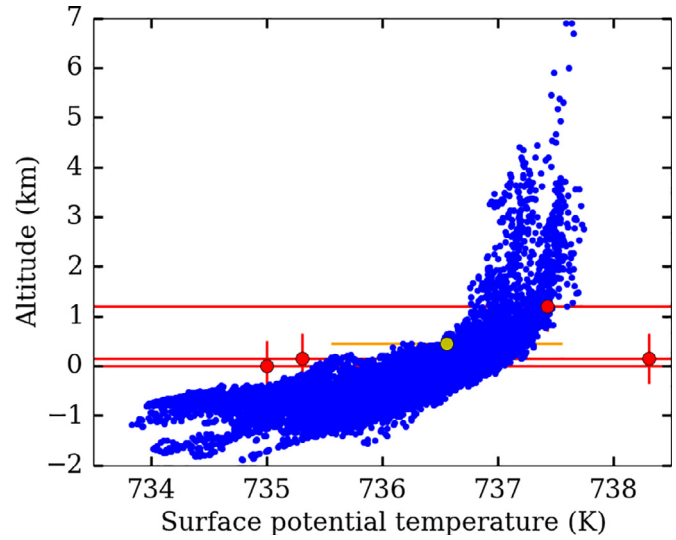

Fig. 3. Diurnally averaged surface potential temperature (K) as a function of surface elevation for every model grid point, shifted by +11 K to compensate the bias in the GCM temperature structure (blue). Surface potential temperatures computed from measurements by the Venera 9 to 12 probes (Avduevskii et al., 1983) are plotted in red and by the VeGa-2 probe (Linkin et al., 1986) in yellow. (For interpretation of the references to colour in this figure legend, the reader is referred to the web version of this article.)

constant at a given location, with diurnal variations limited to at most 3 K. Because the temperature profile below 30 km altitude is mostly determined by the temperature at the base of the clouds and by neutral stability (Lebonnois et al., 2015), the surface temperature is highly correlated with surface topography (vertical gradient close to adiabatic). The relation between surface potential temperature and surface elevation is shown in Fig. 3. If the surface temperature were controlled only by the adiabatic lapse rate, the potential temperature would be homogeneous on the planet. However, in our GCM simulations, the vertical profile of temperature along the slopes is weakly stable, especially in the deeper plains. This behavior may be in agreement with in-situ surface measurements, though uncertainties on these measurements are too large to get a good constraint. The offset between the modeled surface temperatures and observed values is around 11 K (taken into account for the comparison in Fig. 3).

In the atmospheres of Earth, Mars and even Titan, the diurnal cycle of insolation drives the cycle of the PBL dynamics. The discussion is limited here to the dry atmosphere, without consideration of any latent heat exchange. At night, the cooling of the surface yields a stable PBL, with potential temperature increasing with altitude. During daytime hours, solar heating of the surface induces convective activity that generates a well-mixed PBL wherein potential temperature is nearly constant with altitude, up to a stable layer with increasing potential temperature. On Venus, the diurnal cycle of the potential temperature profile is also present. However, this profile is rather different since the deepest region is already close to neutrality, with the potential temperature increasing only very slightly up to 10 km altitude. Stable nocturnal PBL and diurnal near-surface convective activity develop at the bottom of this quasi-neutral region.

The diurnal evolution of the vertical distribution of potential temperature for two different locations on the equator (different longitudes and elevations) is shown in Fig. 4. During the night, a stable PBL is present, due to surface temperature decreasing through infrared cooling of the surface to the atmosphere. During the day, the potential temperature becomes vertically mixed over a layer that depends on local time. This mixing is the result of convective activity.

To explore the roles of radiative forcing and regional dynamical processes in shaping the potential temperature profile below 10 km, 1-

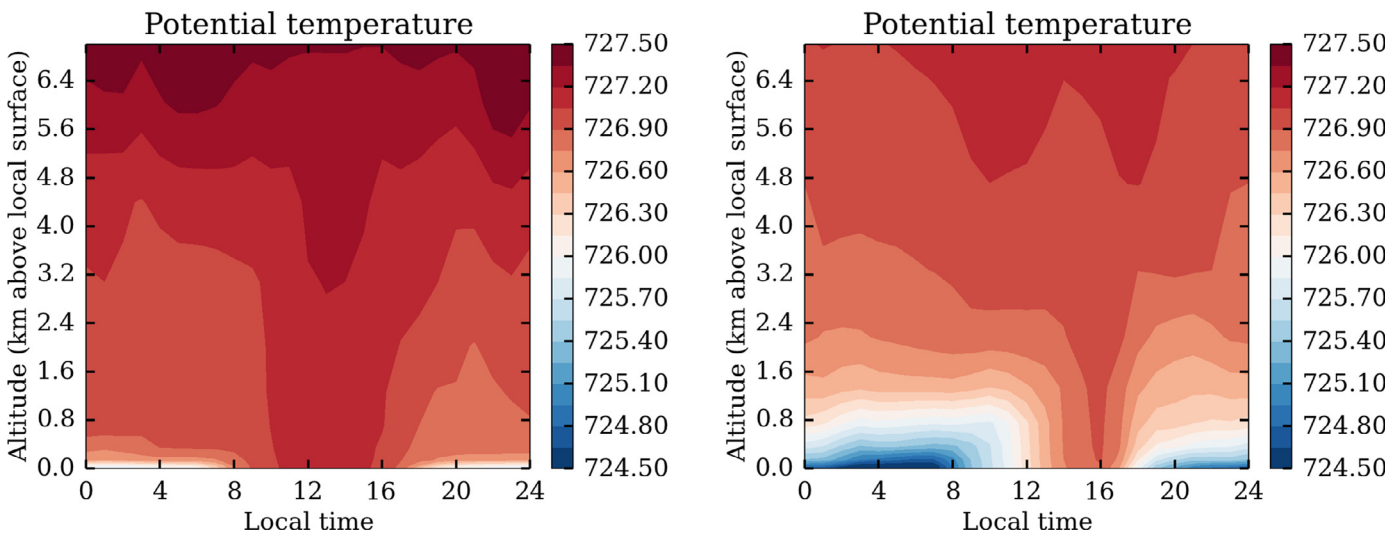

Fig. 4. Potential temperature variations with local time at (left) 92E/equator (surface pressure 74.1 bars) and (right) 0E/equator (surface pressure 94.6 bars).

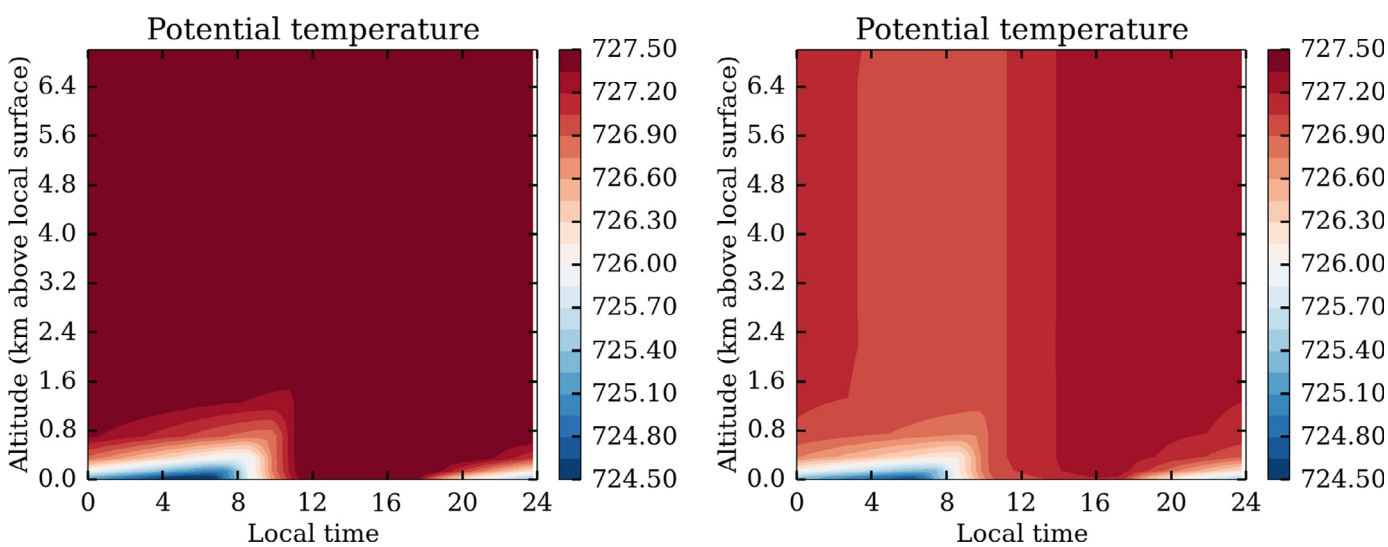

Fig. 5. Same as Fig. 4, but obtained with a 1-dimensional simulations, after 2 Venus days: potential temperature variations with local time at (left) 92E/equator (surface pressure 74.1 bars) and (right) 0E/equator (surface pressure 94.6 bars).

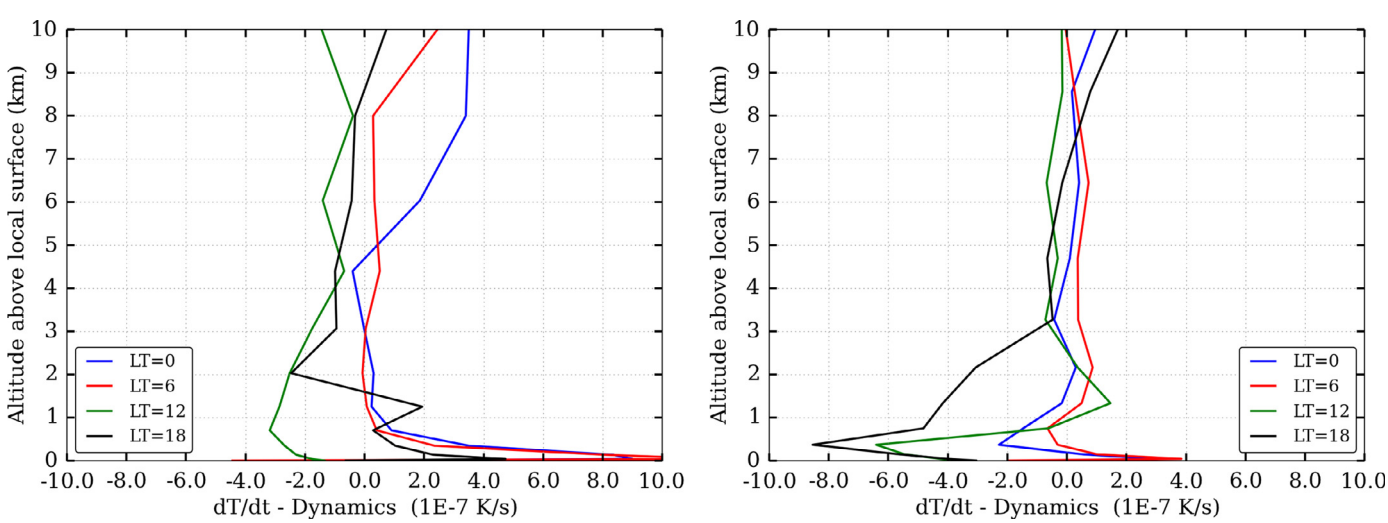

Fig. 6. Atmospheric dynamical heating rates at 4 different local times, at (left) 92E/equator (surface pressure 74.1 bars) and 0E/equator (surface pressure 94.6 bars).

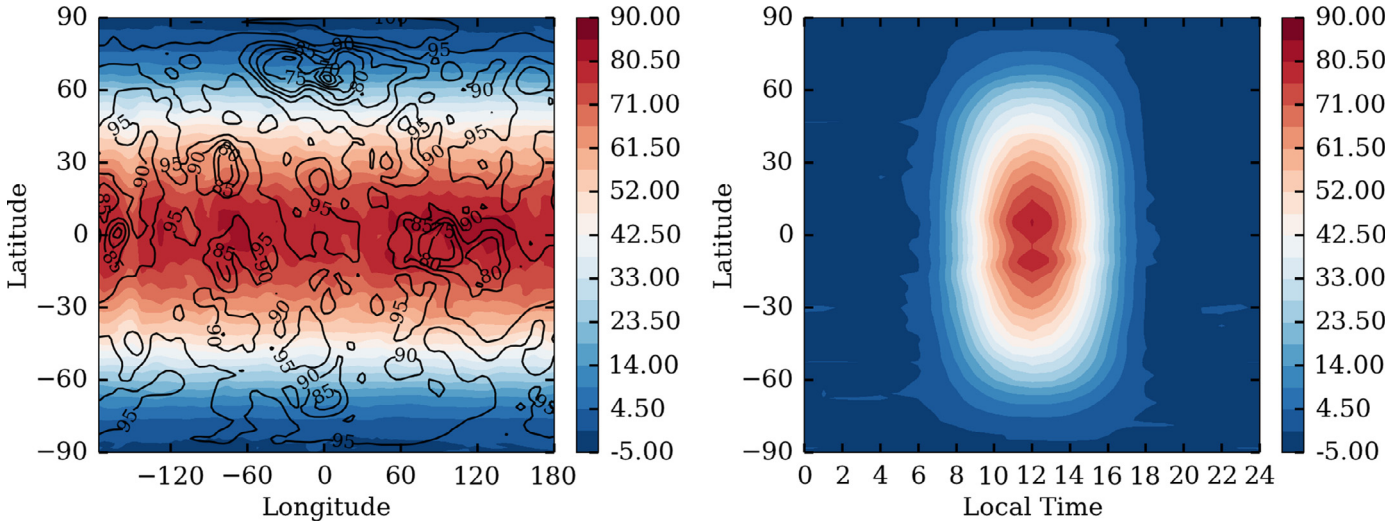

Fig. 7. Sensible heat flux in W/m^2 (positive for upward direction): (left) at noon everywhere, with surface pressure contours (bar); (right) as a function of local time at 60E longitude.

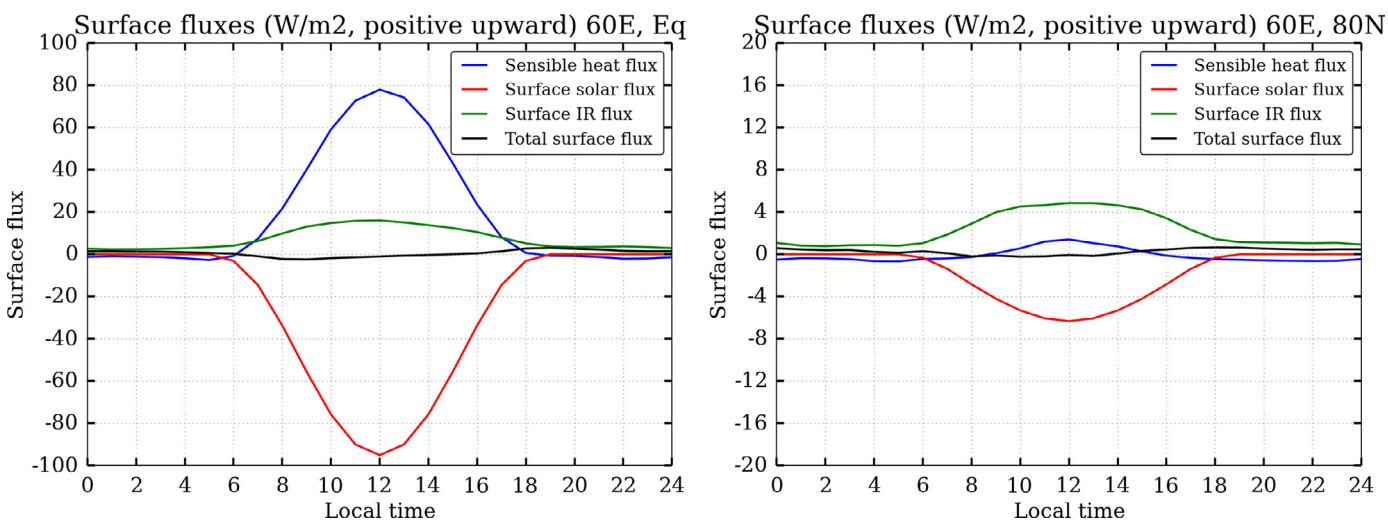

Fig. 8. Surface heat fluxes as a function of local time at (left) 60E/equator and (right) 60E/80N, in W/m2 (positive for upward direction).

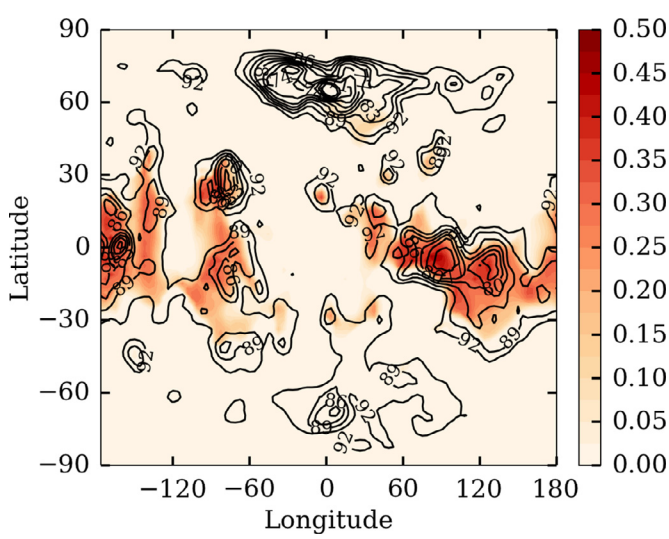

Fig. 9. Turbulent mixing coefficient (in m^2/s) at 2 km above surface at noon everywhere, with surface pressure contours (bars).

dimensional simulations were run at several locations at the equator. Fig. 5 shows the potential temperature evolution in the 1-dimensional runs at the same locations as in Fig. 4, obtained after 2 Venus days (initial state is the GCM profile). These profiles are slightly warmer than in the GCM; large-scale dynamics therefore has a role in slightly cooling the lowest 5 km above the surface. This is confirmed in Fig. 6: dynamics tends to cool the deeper atmosphere during daytime hours. This affects the vertical profile of potential temperature, with regional variations: it tends to be more stable in plains than at high elevations. In Fig. 4, the two cases that are presented show different vertical variations of the potential temperature (mainly the depth of the daytime mixed region). But the same two cases are very similar in Fig. 5, i.e., in the 1-dimensional simulations. This illustrates another impact of large-scale dynamics related to topography, the depth of the convective activity, that is discussed in the next sections.

4. Variability of convective activity

The temporal and spatial variability of the convective activity in the PBL is investigated through an analysis of the sensible heat flux at the surface and of the convective flux.

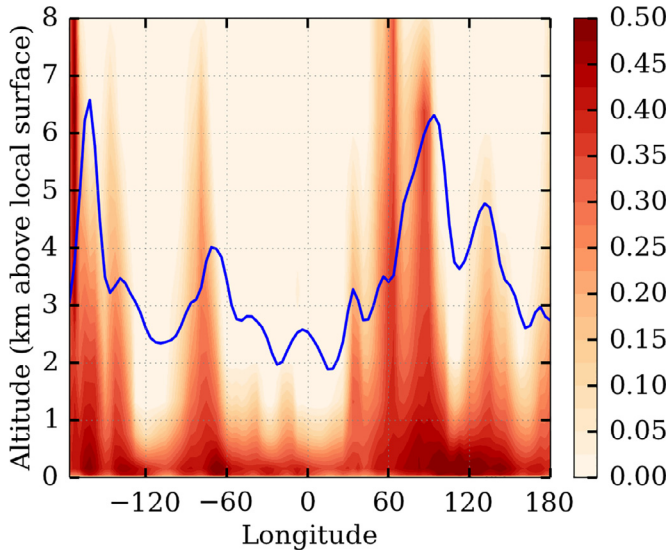

Fig. 10. Turbulent mixing coefficient (in m^2/s) as a function of longitude along the equator, at noon everywhere. Surface elevation is indicated by the blue line (with respect to a radius of 6048 km, to offset it in the figure). (For interpretation of the references to colour in this figure legend, the reader is referred to the web version of this article.)

4.1. Sensible heat flux

The surface sensible heat flux H_s is the turbulent and conductive heat exchanged between the surface and the bottom of the planetary boundary layer. The variations of the sensible heat flux in the GCM simulation are shown in Fig. 7. The diurnal cycle is clear, with a maximum sensible heat flux at noon (12LT) and at low latitudes. This results from a correlation with the solar flux, as also seen in Fig. 8. At high latitudes, solar heating of the surface is mostly compensated by infrared cooling and no convective activity is predicted.

4.2. Correlation with topography

In Fig. 4, the vertical extent of the region with almost uniform potential temperature at noon (correlated with vertical mixing) is different at the two locations. To explore the strength and vertical extent of the modeled convective activity, the distribution of the turbulent mixing coefficient computed by the PBL parameterization scheme is studied. This coefficient is related to the turbulent kinetic energy, as detailed in Hourdin et al. (2002), Appendix B. Fig. 9 shows the map of the maximum value (obtained at noon, LT = 12h) of this mixing coefficient 2 km above the surface. A correlation between the strength of the convective activity and the topography appears at low to mid latitudes, where the sensible heat flux is most active.

This variation of the thickness of the noon convective layer with topography is further illustrated in Fig. 10, showing the maximum mixing coefficient along the equator (at LT = 12h everywhere), with the topographic profile also plotted. The diurnal variations of the convective activity are illustrated for two different locations along this profile in Fig. 11.

Such a correlation with topography is not observed on Earth, but is known on Mars (Spiga et al., 2010). The evolution of the potential temperature in the PBL is driven by the second law of thermodynamics. On Mars, taking into account several approximations, such as neglecting heat conduction, as well as large-scale vertical advection terms, the variation of the mixed-layer potential temperature θ may be written as (Spiga et al., 2010):

$$\frac{\delta\theta}{\delta t} = -\frac{\delta < w'\theta' >}{\delta z} + (J_{SW} + J_{LW})/\Pi, \tag{1}$$

where $\Pi = (p/p_{ref})^{\kappa}$ with p the pressure, p_{ref} a reference surface pressure and $\kappa = R/c_p$ (c_p is the specific heat capacity at constant pressure), $\frac{\delta < w'\theta' >}{\delta z}$ represents the divergence of the convective heat flux (q' denotes a deviation from the averaged quantity $< q >$), and J_{SW} and J_{LW} are the solar heating and infrared cooling rates (in K/s). In the Martian atmosphere, the radiative heating rates are dominant in the energy budget of the convective layer, with surface temperatures that do not depend on altitude. A pressure effect is obtained for similar solar heating and IR cooling rates due to Π in Eq. (1), as demonstrated in Spiga et al. (2010). In the Earth's deserts, the convective term in Eq. (1) is dominant over solar and infrared heating rates, so no effect due to surface pressure occurs.

In the case of Venus, as on Earth, the dominant term is the convective term, with negligible solar and IR heating rates. However, as it will be shown below, the large-scale advection term is not negligible on Venus. Therefore, Eq. (1) applies only to the 1-dimensional simulations. In this case, a very small topographical effect is obtained in the intensity of the convection (not shown), though there is a correlation between surface solar flux, sensible heat flux expressed as $H_s/(\rho c_p)$, and

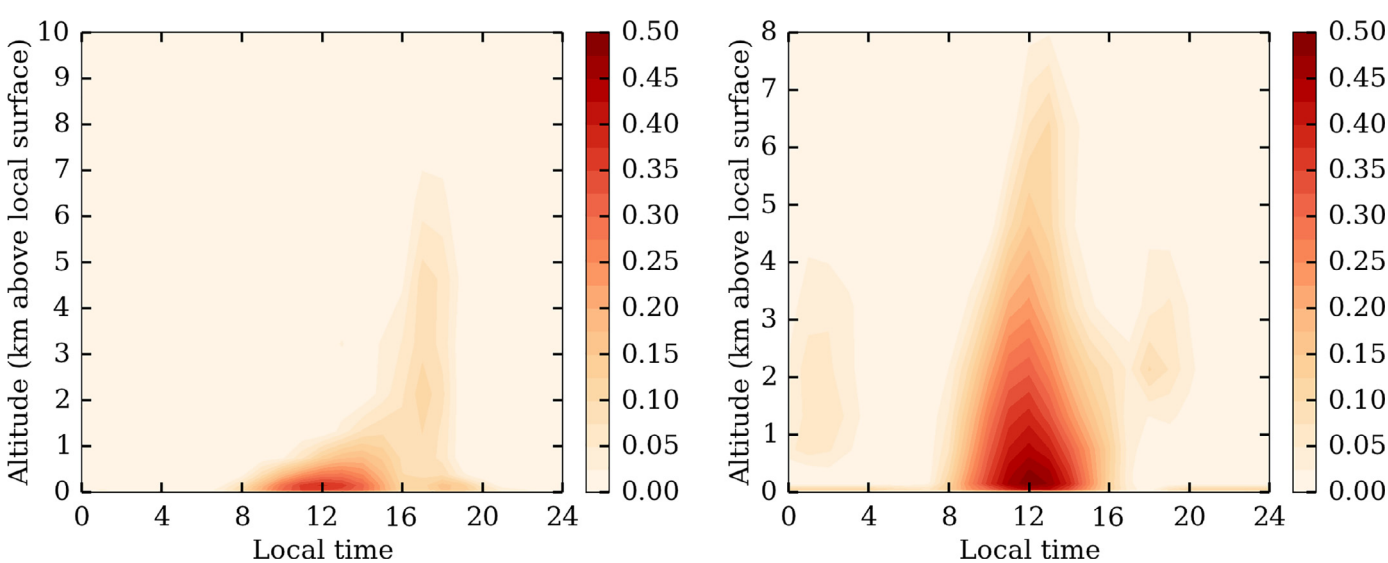

Fig. 11. Turbulent mixing coefficient (in m^2/s) as a function of LT at (left) 0E/equator (surface pressure 94.6 bars) and (right) 92E/equator (surface pressure 74.1 bars).

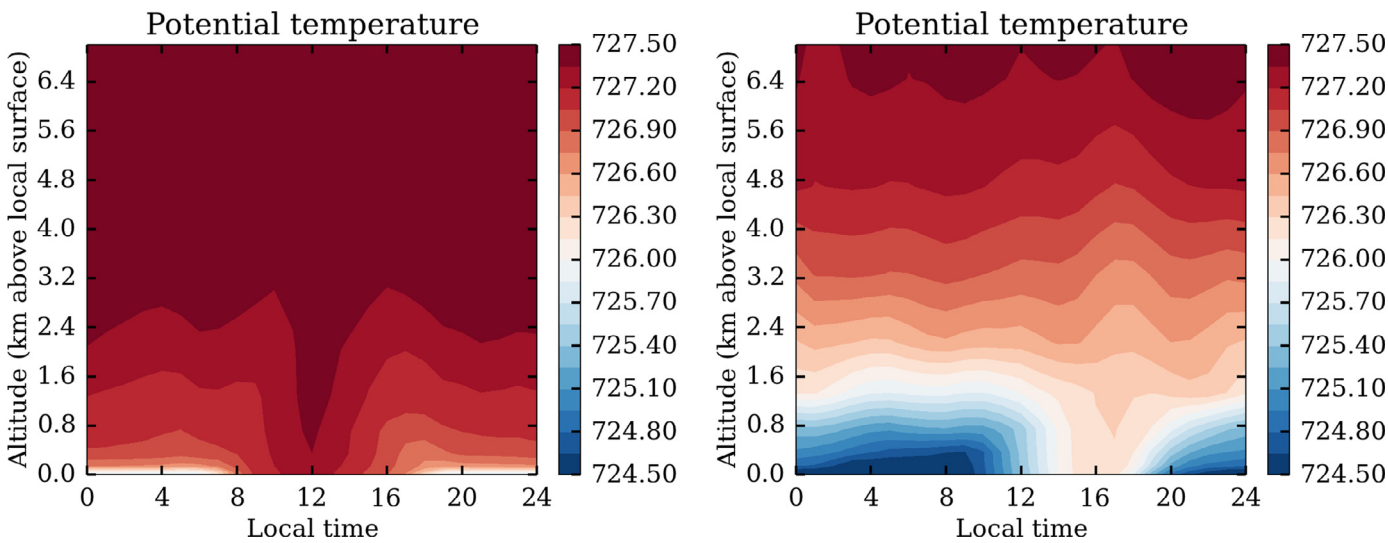

Fig. 12. Same as Fig. 4, but with N_2 variations: potential temperature variations with local time at (left) 92E/equator (surface pressure 74.1 bars) and (right) 0E/equator (surface pressure 94.6 bars).

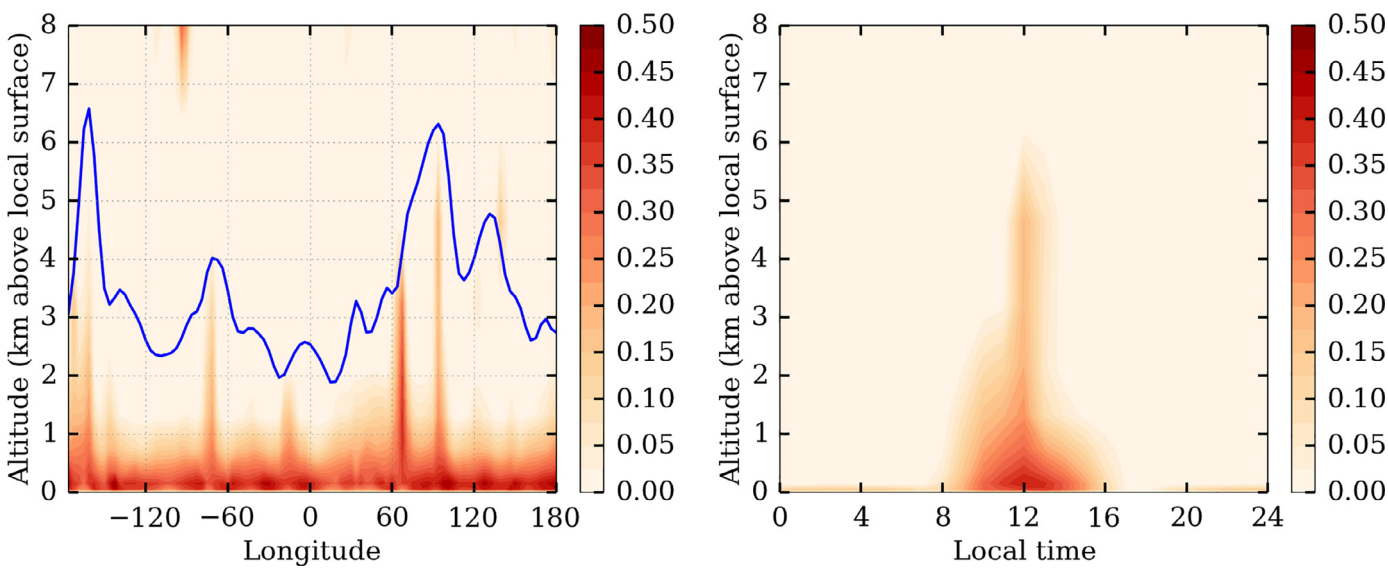

Fig. 13. Same as Fig. 10 and Fig. 11 (right), but with N_2 variations: turbulent mixing coefficient (in m^2/s) (right) as a function of longitude along the equator, at noon everywhere (surface elevation in blue); (left) as a function of LT at 92E/equator (surface pressure 74.1 bars). (For interpretation of the references to colour in this figure legend, the reader is referred to the web version of this article.)

elevation. On Venus, unlike on Mars, the correlation with topography seen in Fig. 9 is therefore not related to topography itself (i.e., surface pressure), but to the dynamics associated with topography. In fact, in Figs. 9 and 10, the maxima of convective activity appear to be located on the western flanks of topographic highs. The reason for this correlation is to be found in the near-surface circulation, as demonstrated in Section 5.

4.3. Impact of the possible gradient of nitrogen mixing ratio

When this gradient is taken into account in the GCM simulation, it affects the vertical extension of the convective layer above topographical features. The stability of the 0–10 km altitude layer is slightly increased by the change in composition, as seen in Fig. 12 compared to Fig. 4, though the overall dynamics and circulation are barely affected. The layer is then less easy to destabilize and for a similar energy balance and similar large-scale wind conditions, the convective activity reaches lower altitudes (Fig. 13, compared to Figs. 10 and 11).

5. Slope winds at the surface of Venus

5.1. Properties

Very few data are available to constrain near-surface winds, mostly measurements by the Venera (e.g. Avduevskii et al., 1977; Golitsyn, 1978) and Pioneer-Venus (Counselman et al., 1980) probes, as well as analyses of aeolian features in Magellan images (Greeley et al., 1994; 1995). However, Lorenz (2016) presented an analysis of these sparse constraints to propose a probability distribution of the near-surface winds, showing that the datasets were compatible with near-surface winds less than 0.7 m/s half the time, and an upper limit of 1.8 m/s (with a probability that the wind is lower of 99%), or up to 2.2 m/s if the upper limits of the measurements were taken into account. In the first layer of the GCM, 10 m above the surface, horizontal winds have an upper limit around 1.5 m/s, with temporally averaged values ranging roughly from 0.2 to 0.6 m/s depending on the location (values up to 1 m/s in the vicinity of the flanks of Ishtar Terra). This appears to be fully compatible with the analysis provided by Lorenz (2016).

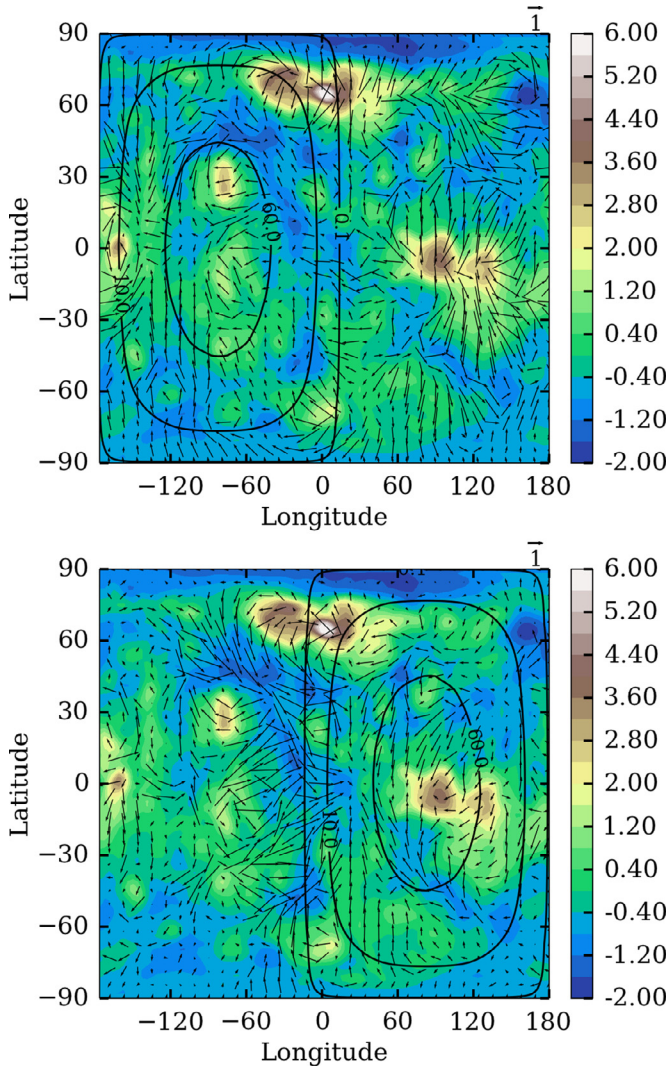

Fig. 14. Maps of the winds at 150 m altitude above the surface (vectors, in m/s) at two different time steps. Contours represent the solar flux received at the surface (in W/m^2). Colors show the elevation of the surface (in km, relative to a radius of 6051 km).

Everywhere, the vertical profile of the horizontal wind is globally increasing with altitude, with westward winds around 3 m/s near 10 km altitude. However, a secondary maximum is present near the surface at an altitude around a few hundred meters, depending on the location and local time. The distribution of these near-surface winds is illustrated in Fig. 14, at 150 m altitude. A complete comparison of these modeled winds with constraints from Magellan data (Greeley et al., 1994; 1995) is not straightforward, as it may depend on the local topography, on the influence of the diurnal cycle, and on the formation mechanisms of the surface features. In the model, on the night side, strong katabatic winds are mostly flowing down the slopes. On the day side, the winds are reversing and anabatic winds are going up the slopes. A westward component is added to this up-slope tendency, maybe due to westward winds from upper layers unblocked by topography. This yields some convergence of the wind on the westward flanks of the mountains, as illustrated for Beta Regio in Fig. 15. In a previous GCM study with topography and diurnal cycle (Yamamoto and Takahashi, 2009), a significant increase in the eddy-component of the near-surface winds was also obtained.

5.2. Relation to the near-surface thermal structure

The potential temperature profiles for two locations, one on top of Beta Regio and one down its eastern flank, at noon and midnight local times are shown in Fig. 16, on the same altitude scale. During the night, the potential temperature is significantly colder at the surface on the mountain slopes than at the same pressure level in the atmosphere away from the surface. This slope-induced baroclinicity drives the nighttime katabatic winds. During daytime, the reverse is true: the surface on the slopes is slightly warmer than the atmosphere at the same pressure level, inducing anabatic winds.

The tendencies on temperature due to the circulation are illustrated in Fig. 6. At night on highlands, the circulation tends to bring relatively warm air to replace the near-surface cold air transported downward by the katabatic winds, inducing heating. The near-surface adiabatic heating associated with these downward katabatic winds is stronger near the bottom of slopes. However, some cooling is present in the lowest elevation plains below 1 km altitude (e.g., Fig. 6, right). During daytime, cooling in the lowlands is also visible, explaining the correlation between topography and surface potential temperature, as discussed in Section 3.

Comparison between Earth and Martian katabatic winds was discussed by Spiga (2011). The slope-buoyancy term (Eq. 2 of Spiga, 2011) leads to stronger katabatic winds for higher surface temperature inversions and higher gravity, though on Earth these conditions are not sufficient and the presence of katabatic winds is observed only in very stable conditions with weak ambient flow perturbations, such as over the Antarctic continent. On Mars, winds are larger because of the strong near-surface inversion caused by the radiative timescales. On Venus, nighttime stability becomes large near the surface, with weak ambient

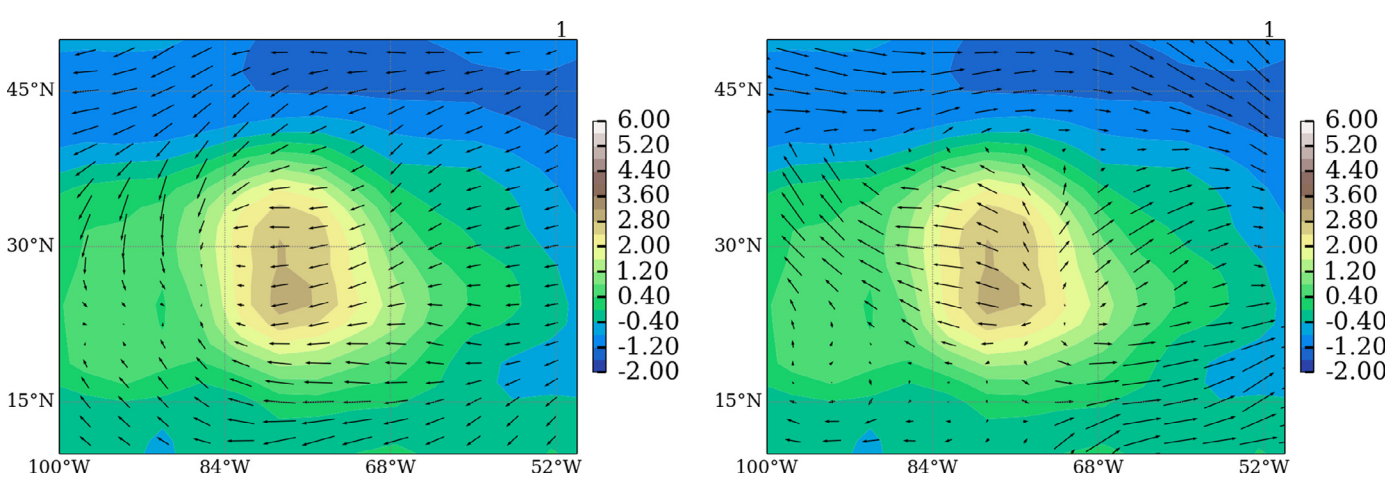

Fig. 15. Same as Fig. 14, but zoomed on Beta Regio. Local time over the area is roughly (left) noon (LT = 12) and (right) midnight (LT = 0).

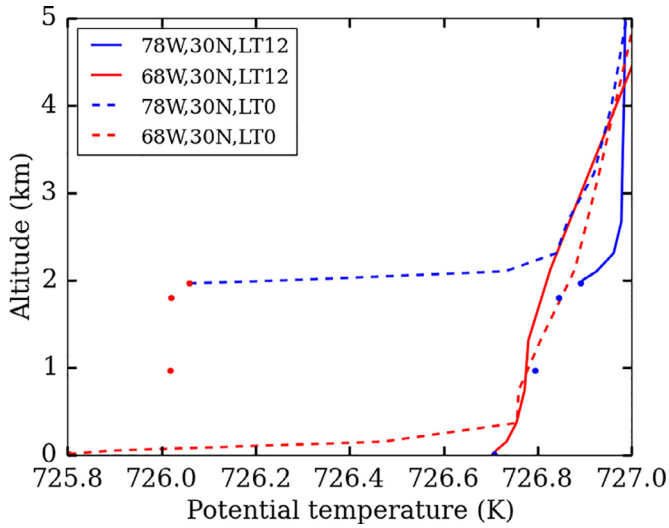

Fig. 16. Vertical profiles of the potential temperature at two different locations, one on top of Beta Regio (78W, 30N, blue lines) and one in the plain down the eastern flank of Beta Regio (68W, 30N, red lines), and at two different local times (noon: LT12, solid lines; midnight: LT0, dashed lines). The surface potential temperatures between these two locations are plotted as dots (red for midnight, blue for noon). Altitude is indicated here with respect to the elevation of the lower location. (For interpretation of the references to colour in this figure legend, the reader is referred to the web version of this article.)

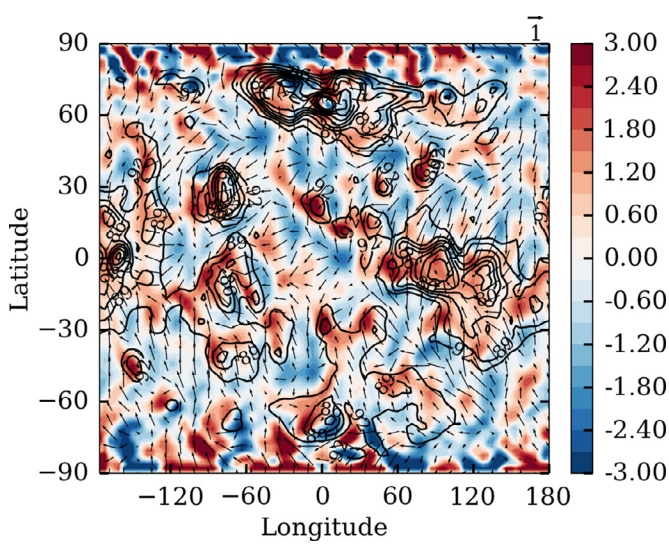

Fig. 17. Horizontal wind convergence (colors, in 10^{-6} s^{-1}) taken at LT12 everywhere, at roughly 150 m above the surface, with wind direction as vectors, and surface pressure contours (bars).

winds, which favors development of strong katabatic winds. An upper limit for the acceleration of the winds along the slope due to this baroclinicity is taken from Eq. 2 in Spiga (2011): it involves the average slope α, the temperature inversion ΔT and the averaged near-surface temperature $< T >$. According to Fig. 16, with the two locations separated by roughly 1000 km, α is around 2×10^{-3}, $< T >$ is around 726 K and ΔT is roughly 0.8 K for midnight and 0.05 K for noon. This gives accelerations of up to nearly 2×10^{-5} m/s^2 at midnight and 1.2×10^{-6} m/s^2 at noon. Given the duration of one Venusian hour in local time (which is 4.2×10^5s), this means that katabatic winds may easily reach several m/s, as obtained in the simulation, while anabatic winds are less intense and more affected by vertical mixing associated with convective motions in the PBL.

5.3. Impact on the daytime convective PBL

The convergence of the daytime anabatic winds is shown around 150 m altitude in Fig. 17, with local time fixed to noon everywhere. This convergence of horizontal winds in the near-surface layers induces upwelling of air near topographical features, and more specifically along the western slopes of these elevated regions, as illustrated in Fig. 18, that shows the vertical winds at 2 km altitude. A strong correlation is clearly seen between these upward motions and the regions where convective activity reaches higher altitudes (Fig. 9), though limited to the mid-latitudes because of the dependence of the convective activity and sensible heat flux on solar flux, as discussed previously.

The impact of the vertical wind in the environment on the vertical extension of the PBL is described, e.g., by Garratt (1992). The temporal evolution $\dot{z}_i$ of the PBL depth z_i is to first order the sum of the vertical entrainment velocity w_e (related to buoyancy and convective turbulence) and the background vertical velocity w_b (related to regional and large-scale ascending or subsiding motions). The latter term explains how, even in the Martian environment where turbulent plumes in the PBL are very powerful, regional circulations can dramatically impact the depth of the convective PBL. This is exemplified by Tyler and Barnes (2015) in the case of Gale Crater, the Curiosity rover's landing site. There, the daytime subsidence over crater floors (as a result of slope circulation) produces adiabatic warming, which inhibits the growth of the convective boundary layer by forming a capping inversion. Similar phenomena are at play on Venus, where regional upwelling associated with anabatic winds during noon hours causes the PBL to be deeper above the western slopes of elevated regions: as an example, upwelling vertical winds of the order of 5 mm/s over 1 Venusian hour (1Vh = 4.2×10^5s) can increase the vertical depth of the PBL by 2 km, which is consistent with the value of $\dot{z}_i$ seen in Fig. 11 (right panel).

6. Conclusion

The possible structure and characteristics of Venus' planetary boundary layer have been investigated with general circulation simulations based on the IPSL Venus GCM. Though the PBL is modeled based on a parameterization in this large-scale climate model, it allows us to describe the dominant features of the dynamics of the near-surface regions.

The model predicts a diurnal cycle for the PBL activity, with a stable nocturnal PBL while convective activity develops during daytime. The diurnal convective PBL is strongly correlated with surface solar flux and is maximum around noon and in low latitude regions. It typically reaches less than 2 km above the surface, but vertical extension is much higher over high elevations, and more precisely over the western flanks of elevated terrains. The surface winds undergo a diurnal cycle, with katabatic winds at night and anabatic winds during the day. Convergence of these daytime anabatic winds induces upward winds, that are responsible for the correlation between topographical features and larger vertical extension of the PBL.

Caution must be kept, as models are always subject to uncertainties and assumptions. In particular, these simulations are sensitive to the radiative heating rates in the deep atmosphere, which are poorly constrained. LES simulations could help validate the behavior of the PBL parameterization. However, large-scale dynamics has to be taken into account in these models, since the GCM shows that its thermal impact is a crucial term in the potential temperature vertical profile, and the background vertical wind is strongly affecting the development of the convection.

Additional data are crucially needed from the deepest 10 km above the surface, better to understand this region, the interface between surface and atmosphere. Accurate temperature and radiative fluxes profiles are essentials to validate the predictions of models.

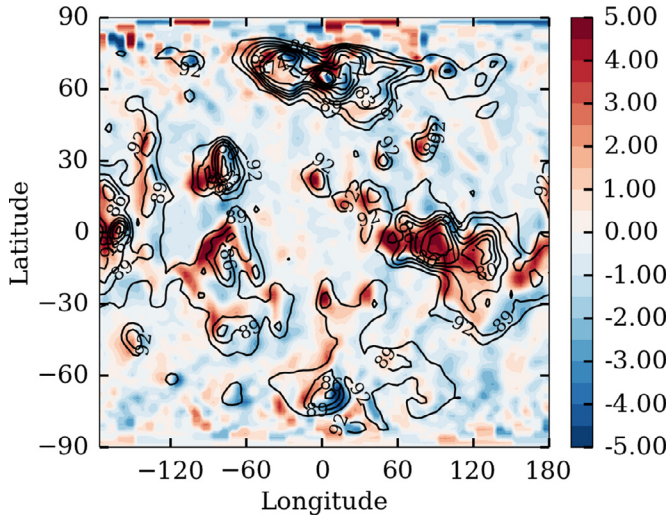

Fig. 18. Vertical winds (in mm/s) taken at LT12 everywhere, at roughly 2 km above the surface, with surface pressure contours (bars). Positive winds are upward.

Acknowledgments

S.L., F.F. and A.S. acknowledge the support of the Centre National d'Etudes Spatiales. G.S. acknowledges the support of the Keck Institute for Space Studies under the project "Techniques and technologies for investigating the interior structure of Venus". GCM simulations were done at CINES, France, under the project n°11167.

Supplementary material

Supplementary material associated with this article can be found, in the online version, at doi:10.1016/j.icarus.2018.06.006

References

Avduevskii, V.S., Marov, M.Y., Kulikov, Y.N., Shari, V.P., Gorbachevskii, A.Y., Uspenskii, G.R., Cheremukhina, Z.P., 1983. Structure and parameters of the Venus atmosphere according to Venera probe data. In: Hunten, D.M., Colin, L., Donahue, T.M., Moroz, V.I. (Eds.), VenusUniv. of Arizona Press, pp. 280–298.

Avduevskii, V.S., Vishnevetskii, S.L., Golov, I.A., Karpeiskii, I.I., Lavrov, A.D., Likhushin, V.I., Marov, M.I., Melnikov, D.A., Pomogin, N.I., Pronina, N.N., 1977. Measurement of wind velocity on the surface of Venus during the operation of stations Venera 9 and Venera 10. Cosmic Res. 14, 710–713.

Charnay, B., Lebonnois, S., 2012. Two boundary layers in Titan's lower troposphere inferred from a climate model. Nat. Geosci. 5, 106–109.

Counselman, C.C., Gourevitch, S.A., King, R.W., Loriot, G.B., Ginsberg, E.S., 1980. Zonal and meridional circulation of the lower atmosphere of Venus determined by radio interferometry. J. Geophys. Res. 85, 8026–8030.

Dobrovolskis, A.R., 1983. Atmospheric tides on Venus. III - the planetary boundary layer. Icarus 56, 165–175.

Dobrovolskis, A.R., 1993. Atmospheric tides on Venus. IV - topographic winds and sediment transport. Icarus 103, 276–289.

Eymet, V., Fournier, R., Dufresne, J.L., Lebonnois, S., Hourdin, F., Bullock, M.A., 2009. Net-exchange parameterization of the thermal infrared radiative transfer in Venus' atmosphere. J. Geophys. Res. 114. E11008

Garate-Lopez, I., Lebonnois, S., 2018. Latitudinal variation of clouds' structure responsible for Venus cold collar. Icarus. http://dx.doi.org/10.1016/j.icarus.2018.05.011.

Garratt, J.R., 1992. The Atmospheric Boundary Layer. Cambridge Univ. Press, New York.

Garratt, J.R., 1994. Review: the atmospheric boundary layer. Earth Sci. Rev. 37, 89–134.

Golitsyn, G.S., 1978. Estimates of the turbulent state of the atmosphere near the surface of Venus from the data of Venera 9 and Venera 10. Cosmic Res. 16, 125–127.

Greeley, R., Bender, K., Thomas, P.E., Schubert, G., Limonadi, D., Weitz, C.M., 1995. Wind-related features and processes on Venus: summary of magellan results. Icarus 115, 399–420.

Greeley, R., Marshall, J.R., Clemens, D., Dobrovolskis, A.R., Pollack, J.B., 1991. Venus - concentrations of radar-reflective minerals by wind. Icarus 90, 123–128.

Greeley, R., Schubert, G., Limonadi, D., Bender, K.C., Newman, W.I., Thomas, P.E., Weitz, C.M., Wall, S.D., 1994. Wind streaks on Venus: clues to atmospheric circulation. Science 263, 358–361.

Haus, R., Kappel, D., Arnold, G., 2014. Atmospheric thermal structure and cloud features in the southern hemisphere of Venus as retrieved from VIRTIS/VEX radiation measurements. Icarus 232, 232–248.

Haus, R., Kappel, D., Arnold, G., 2015. Radiative heating and cooling in the middle and lower atmosphere of Venus and responses to atmospheric and spectroscopic parameter variations. Planet. Space Sci. 117, 262–294.

Hess, S.L., Henry, R.M., Leovy, C.B., Tillman, J.E., Ryan, J.A., 1977. Meteorological results from the surface of Mars - Viking 1 and 2. J. Geophys. Res. 82, 4559–4574.

Hinson, D.P., Pätzold, M., Tellmann, S., Häusler, B., Tyler, G.L., 2008. The depth of the convective boundary layer on Mars. Icarus 198, 57–66.

Hourdin, F., Couvreux, F., Menut, L., 2002. Parameterization of the dry convective boundary layer based on a mass flux representation of thermals. J. Atmos. Sci. 59, 1105–1123.

Lebonnois, S., Eymet, V., Lee, C., Vatant d'Ollone, J., 2015. Analysis of the radiative budget of Venus atmosphere based on infrared net exchange rate formalism. J. Geophys. Res. Planets 120, 1186–1200.

Lebonnois, S., Hourdin, F., Eymet, V., Crespin, A., Fournier, R., Forget, F., 2010. Superrotation of Venus' atmosphere analysed with a full general circulation model. J. Geophys. Res. 115. E06006

Lebonnois, S., Schubert, G., 2017. The deep atmosphere of Venus and the possible role of density-driven separation of CO_2 and N_2. Nat. Geosci. 10, 473–477.

Lebonnois, S., Sugimoto, N., Gilli, G., 2016. Wave analysis in the atmosphere of Venus below 100-km altitude, simulated by the LMD venus GCM. Icarus 278, 38–51.

Linkin, V.M., Blamont, J.E., Lipatov, A.N., Devyatkin, S.I., D'yachkov, A.V., Ignatova, S.P., Kerzhanovich, V.V., Khlyustova, L.I., Malique, C., Sanotskil, Y.V., Shurupov, A.A., Stadnyk, B.I., Stolyarchuk, P.G., Terterashvili, A.V., 1986. Vertical thermal structure in the Venus atmosphere from provisional Vega 2 temperature and pressure data. Sov. Astron. Lett. 12, 40–42.

Lorenz, R.D., 2016. Surface winds on Venus: probability distribution from in-situ measurements. Icarus 264, 311–315.

Mellor, G.L., Yamada, T., 1982. Development of a turbulent closure model for geophysical fluid problems. Rev. Geophys. Space Phys. 20, 851–875.

Mueller, N., Helbert, J., Hashimoto, G.L., Tsang, C., Erard, S., Piccioni, G., Drossart, P., 2009. Venus surface thermal emission at 1 μm in VIRTIS imaging observations: evidence for variation of crust and mantle differentiation conditions. J. Geophys. Res. 114. E00B39

Saunders, R.S., Wall, S.D., Dobrovolskis, A.R., Greeley, R., 1990. Large-scale patterns of eolian sediment transport on Venus - predictions for magellan. Geophys. Res. Lett. 17, 1365–1368.

Spiga, A., 2011. Elements of comparison between martian and terrestrial mesoscale meteorological phenomena: katabatic winds and boundary layer convection. Planet. Space Sci. 59, 915–922.

Spiga, A., Forget, F., Lewis, S.R., Hinson, D.P., 2010. Structure and dynamics of the convective boundary layer on Mars as inferred from large-eddy simulations and remote-sensing measurements. Q. J. R. Meteorol. Soc. 136, 414–428.

Spiga, A., Forget, F., Madeleine, J.B., Montabone, L., Lewis, S.R., Millour, E., 2011. The impact of martian mesoscale winds on surface temperature and on the determination of thermal inertia. Icarus 212, 504–519.

Tyler, D., Barnes, J.R., 2015. Convergent crater circulations on Mars: influence on the surface pressure cycle and the depth of the convective boundary layer. Geophys. Res. Lett. 42, 7343–7350.

Wang, M.Z., Lu, H., Ming, H., Zhang, J., 2016. Vertical structure of summer clear-sky atmospheric boundary layer over the hinterland and southern margin of Taklamakan desert. Meteorol. Appl. 23, 438–447.

Yamamoto, M., 2011. Microscale simulations of Venus' convective adjustment and mixing near the surface: thermal and material transport processes. Icarus 211, 993–1006.

Yamamoto, M., Takahashi, M., 2009. Influences of Venus' topography on fully developed superrotation and near-surface flow. Earth Planets Space 61. E45–e48